



Advanced microstructural characterisation of cast ATI 718Plus®—effect of homogenisation heat treatments on secondary phases and repair welding behaviour

Fabian Hanning¹ · Abdul Khaliq Khan^{2,3} · Joel Andersson⁴ · Olanrewaju Ojo²

Received: 21 August 2019 / Accepted: 7 January 2020 / Published online: 23 January 2020
© The Author(s) 2020

Abstract

The influence of base metal conditions on the weld cracking behaviour of cast ATI 718Plus® is investigated by comparing 4 h and 24 h dwell time pseudo-hip homogenisation heat treatments at 1120, 1160 and 1190 °C with the as-cast microstructure. Scanning electron microscopy (SEM), X-ray diffraction (XRD) on electrolytically extracted powder and transmission electron microscopy (TEM) were used to identify Nb-rich secondary phases in interdendritic areas as the C14 Laves phase and Nb(Ti) MC-type carbides. All homogenisation heat treatments but the 1120 °C 4-h condition dissolve the Laves phase. A repair welding operation was simulated by linear groove multi-pass manual gas tungsten arc welding (GTAW). The Laves phase containing microstructures resulted in lower total crack length for heat affected zone cracking. Constitutional liquation of Nb(Ti) MC-type carbides is observed as a liquation mechanism in Laves-free microstructure, while thick liquid film formation due to the Laves eutectic melting could reduce the formation of weld cracks in microstructures containing the Laves phase.

Keywords (IIW thesaurus) nickel alloys · Weldability · Repair · GTA welding · Cracking · ATI 718Plus®

1 Introduction

The limiting maximum service temperature of Alloy 718 has in recent years led to the development of derivative alloys with increased thermal stability. One of them is ATI 718Plus®,

providing a 50 °C increase in maximum service temperature by using a modified chemistry to favour the formation of gamma prime phase as main hardening precipitate [1]. Initially, the material has been introduced as a wrought material. A cast version is now available as well, which was developed within the Metals Affordability Initiative programme [2, 3]. The development resulted in a modified chemistry of the cast version, which includes an increased amount of Nb of 6.5 wt% as compared with 5.5 wt% in wrought material. The strong segregation present in castings makes them generally less weldable than wrought material; however, when fabricating large structural components for aerospace applications, welding is often a requirement. Furthermore, imperfections from the casting process may be repaired by welding operations instead of costly full replacements. Cast material is commonly put through a homogenisation heat treatment to obtain a more levelled elemental distribution in the microstructure and to dissolve deleterious secondary phases formed during the casting process. For Nb-bearing alloys such as Alloy 718 and ATI 718Plus®, the brittle Laves phase commonly forms in the interdendritic areas due to Nb segregation. Its low incipient melting point through eutectic reaction can cause formation of liquid at low temperatures. This can lead to the formation of liquation cracks in the heat affected zone

✉ Fabian Hanning
fabian.hanning@chalmers.se

Abdul Khaliq Khan
abdulkhaliq.khan@umanitoba.ca

Joel Andersson
joel.andersson@hv.se

Olanrewaju Ojo
olanrewaju.ojo@umanitoba.ca

¹ Department of Industrial and Materials Science, Chalmers University of Technology, Gothenburg, Sweden

² Department of Mechanical Engineering, University of Manitoba, Winnipeg, Canada

³ Manitoba Institute for Materials, University of Manitoba, Winnipeg, Canada

⁴ Department of Engineering Science, University West, Trollhättan, Sweden

(HAZ) during welding [4]. In previous investigations, the effect of homogenisation heat treatments on the weld cracking behaviour of cast ATI 718Plus® has been investigated, and a positive effect of Nb-rich phases has been reported [5, 6]. The present study aims to provide further insight by advanced microstructural characterisation and identification of the secondary phases present after different homogenisation heat treatments and their effect on weld cracking during repair.

2 Experimental

2.1 Material and heat treatments

The ATI 718Plus® used in this study was in the form of investment cast plates with dimensions of 150 × 60 × 13 mm. The chemical composition is shown in Table 1. In the as-cast condition, the material shows a dendritic microstructure with an average grain size of 1300 ± 200 µm as shown in Fig. 1a. In interdendritic areas, blocky Nb-rich precipitates can be observed as bright areas in SEM backscattered electron (BSE) contrast Fig. 1b. The hardness has been measured to 415 ± 5 HV0.5.

Besides the as-cast material, plates were put through different homogenisation heat treatments. As opposed to wrought material, cast materials can generally be subjected to homogenisation temperatures that are well above the dissolution temperature of secondary carbides, since grain growth is not a concern. The reason for such a heat treatment in Nb-bearing alloys is the dissolution of the detrimental Laves phase, which is a remnant from the casting solidification process, where it forms as residual eutectic liquid. This phase is not stable at nominal alloy composition and can hence be dissolved during prolonged high temperature exposure. This study investigated three homogenisation temperatures, 1120, 1160 and 1190 °C, with dwell times of 4 and 24 h, respectively. These temperatures lie below, at and above the incipient Laves melting temperature of 1160 °C [7]. In an industrial setting, homogenisation heat treatments are commonly carried out in conjunction with hot isostatic pressing (HIP). In this study, all heat treatments have been carried out at ambient pressure in a small lab furnace.

2.2 Repair welding

Manual gas tungsten arc welding (GTAW) was carried out to simulate a repair operation. Each plate was prepared by

machining four linear grooves with the dimensions of 30 × 10 × 10 mm and a bottom radius of 5 mm. The welding operation was carried out by experienced welders, using a tungsten 2% thorium (WT-20) electrode. The welds were shielded by argon with a nozzle gas flow of 8–15 l/min. ATI 718Plus® filler wire with 1.14 mm diameter was used to fill the grooves. Welding was carried out using a wide nozzle, creating a diffuse shielding gas flow. This enables a large electrode stick-out to reach the bottom of the narrow welding grooves. The welding current was set to 140 A with an interpass temperature of approximately 50 °C. It has to be emphasised that the chosen welding procedure represents extreme conditions regarding the weld bead geometry and the heat input. While a typical repair operation would not be carried out this way, the tough welding conditions were selected to provoke crack formation in the material.

2.3 Weld examination and microstructural characterisation

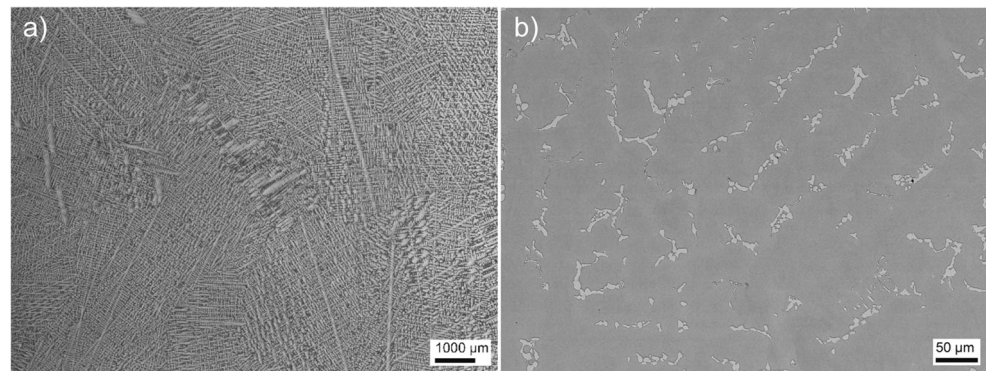
To examine the welds, six cross sections were prepared from each groove, oriented transverse to the welding direction and cut out evenly spaced along the groove length. Samples were mounted in hot mounting resin and subjected to standard automated metallographic preparation. Samples were electrolytically etched using a 10-wt% oxalic acid solution at 3 V DC for 3 to 5 s. Visual inspection of cracks has been carried out using a light optical microscope at × 200 magnification. The length of cracks was measured by following the centreline of the crack. Presented data averages total crack length (TCL) over four welding grooves (i.e. one plate). Microhardness was measured using a Shimadzu HMV-2 microhardness tester with a force of 0.5 kgf (HV0.5). A Leo 1550 FE SEM and a Zeiss Evo 50 SEM, both equipped with Oxford EDS systems, were used to perform electron microscopy on the welded samples. Image analysis for measuring the area fraction of secondary phases has been carried out with ImageJ on 5 SEM images per material condition. Atomic number contrast visible in BSE images was used to distinguish the Laves phase and Nb-rich carbides from the matrix.

To further analyse the secondary phases in the material, both phase extraction, X-ray diffraction (XRD) and TEM, with selected area (SA) diffraction and EDS were used. Powder samples for XRD analysis were produced by electrolytically dissolving the matrix phase in an electrolyte consisting of 100 ml HCl, 900 ml methanol and 17.6 g tartaric acid. A rectangular sample was polarised to 0.1 A/cm². After

Table 1 Chemical composition of cast ATI 718Plus® in wt%

Ni	Cr	Co	Mo	Ti	Al	Fe	Mn	Si	C	B	Nb	W
Bal	20.72	8.34	2.71	0.75	1.50	9.31	0.01	0.04	0.05	0.005	6.02	1.00

Fig. 1 **a** Microstructure of as cast ATI 718Plus[®] showing grain structure. **b** Bright Nb-rich precipitates in SEM BSD contrast



4 h, the extracted powder samples were filtrated using a 0.8- μm filter paper and dried. The method is described in more detail in ASTM E963 [8]. Powder XRD was subsequently carried out using a Bruker D5000 powder diffractometer with 0.01 $^{\circ}\text{C}$ step size and 4 s per step. Peak analysis has been carried out using the PDF 2018+ database.

To examine the alloy by TEM, samples were thinned to 100 μm thickness, followed by dimple grinding and electropolishing in 10:90 methanolic perchloric acid at -40 $^{\circ}\text{C}$ using a Struers Tenupol-3 twinjet polishing machine. The samples were investigated with a Jeol JEM-2100 field emission transmission electron microscope at 200 kV. JmatPro v. 10.1 was used for thermodynamic calculations.

A Gleeble 3800 thermomechanical simulator was used to simulate thermal and loading cycles present in the base metal HAZ during welding. Testing conditions were similar to the hot ductility test (HDT). The testing procedure is described in more detail in [9]. A heating rate of 111 $^{\circ}\text{C}/\text{s}$ was used together with a peak temperature exposure time of 0.003 s and a stroke rate of 55 mm/s. Selected samples were also tested using only the thermal cycling part of the test. Fracture surfaces and cross sections cut out of the centre of test specimens were subsequently analysed using electron microscopy.

3 Results and discussion

3.1 Microstructural characterisation

The grain size was found to be constant over all investigated material conditions, while a significant drop in hardness could be observed for all solution heat-treated samples as compared with the as-cast condition. Grain size and hardness results are shown in Table 2. The change in microstructure after solution heat treatments is shown in Fig. 2, where a reduction in interdendritic secondary phases is clearly visible for all heat-treated samples, albeit the 1120 $^{\circ}\text{C}$ 4 h treatment being less effective than the other conditions. The area fraction of Nb-rich phases as obtained by automatic image analysis is shown in Fig. 3. With an initial amount of 5.2 ± 0.3 area% in the as-

cast material, a baseline amount of ~ 0.5 area% is reached for all but the 1120 $^{\circ}\text{C}$ 4 h heat treatment. JMatPro predicts the equilibrium phase fraction of primary MC-type carbides as 0.47–0.49 wt% for the investigated homogenisation heat treatment temperature range. For a true comparison, the volume fraction would need to be computed from the image analysis results by taking the particle shape into account. This is however not attempted here, and the close apparent agreement of the results with the simulation is rather seen as an indication of what phases are expected to be present in the material.

With further microstructural investigation of precipitates using SEM EDS on as cast material, two distinct precipitate types could be identified in the microstructure. Figure 4 shows EDS spot measurements in an interdendritic area of the as-cast material, together with a BSE image indicating the measurement positions. The bright appearance of the phases in BSE mode indicates high content of heavy elements such as Nb, which is supported by the high measured intensities at the Nb-L α position. A distinct difference in intensity between measurement points further suggests the presence of two separate phases in the interdendritic areas. Nb-rich MC-type carbides are stable phase in ATI 718Plus[®], while the Laves phase is commonly formed in Nb-bearing superalloy castings due to elemental segregation [10].

High resolution FE-SEM imaging shows the presence of small cuboidal precipitates around the presumed Laves phase and MC carbides, Fig. 5. The phase appears to be γ' , which can

Table 2 Grain size and hardness in the base material for different homogenisation heat treatments

Material condition	Grainsize (μm)	Hardness (HV0.5)
As-cast	1290 ± 200	415 ± 5
1120 $^{\circ}\text{C}$	4 h	1370 ± 100
	24 h	1350 ± 280
1160 $^{\circ}\text{C}$	4 h	1290 ± 100
	24 h	1400 ± 230
1190 $^{\circ}\text{C}$	4 h	1290 ± 120
	24 h	1330 ± 200

Fig. 2 Base material microstructure after homogenisation heat treatments. **a** 1120 °C 4 h. **b** 1120 °C 24 h. **c** 1160 °C 4 h. **d** 1160 °C 24 h. **e** 1190 °C 4 h. **f** 1190 °C 24 h

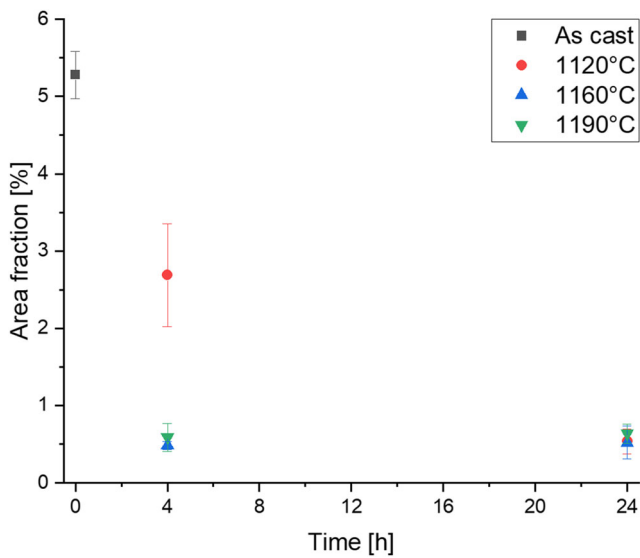
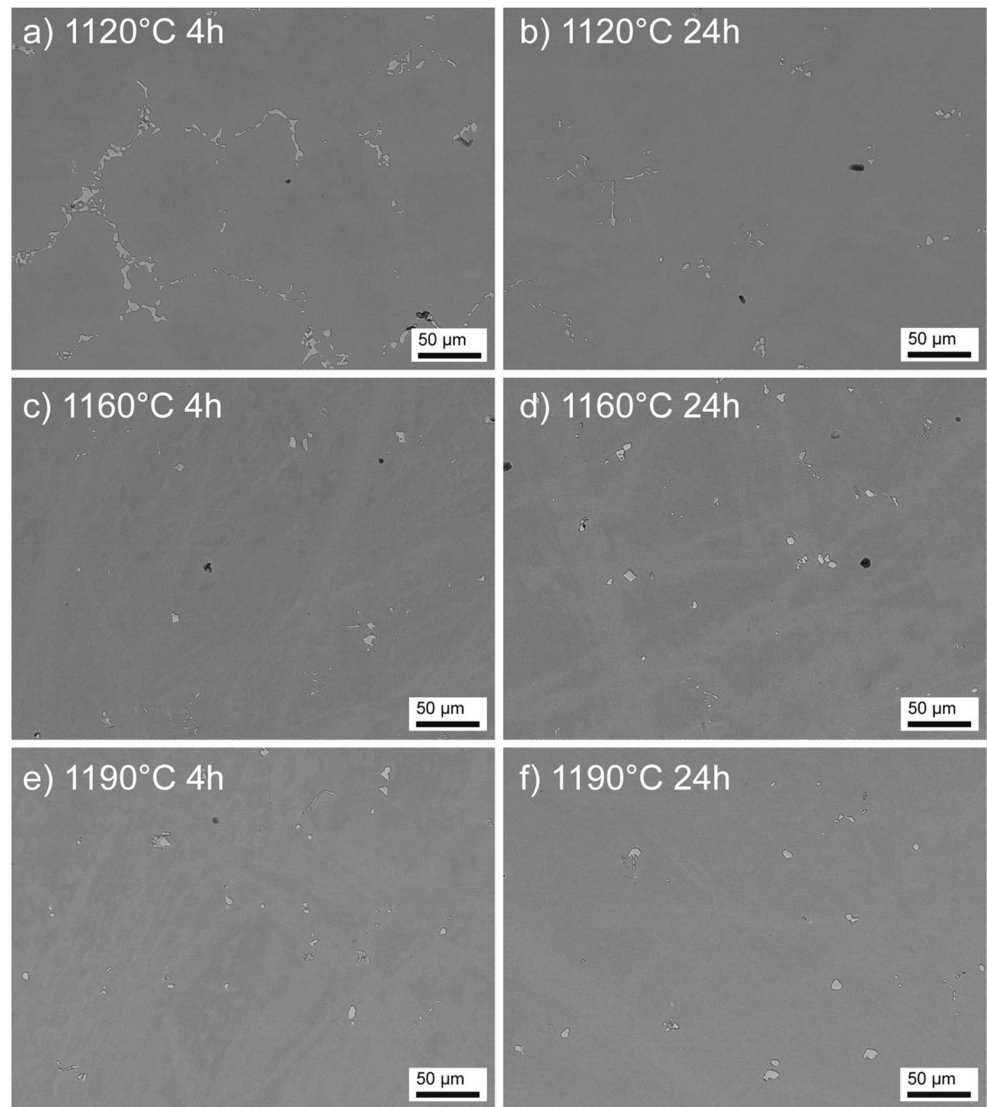


Fig. 3 Area fraction of Nb-rich precipitates after different homogenisation heat treatments, indicating incomplete dissolution for the 1120 °C 4 h heat treatment

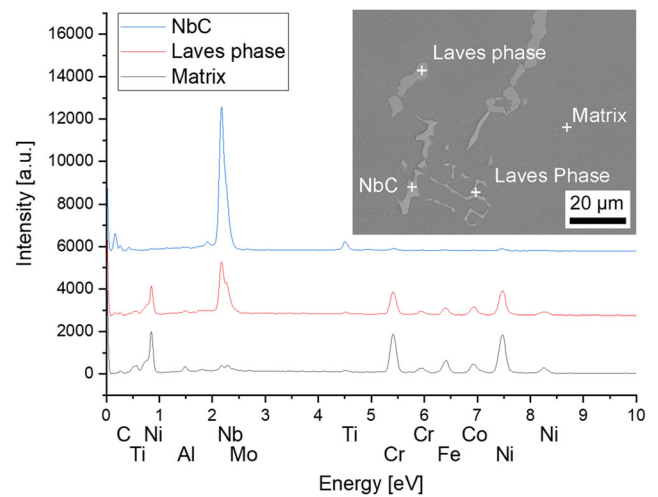


Fig. 4 EDS spot measurements in an interdendritic area of the as-cast material. Distinct differences in Nb L- α indicate the presence of both NbC carbides and Laves phase

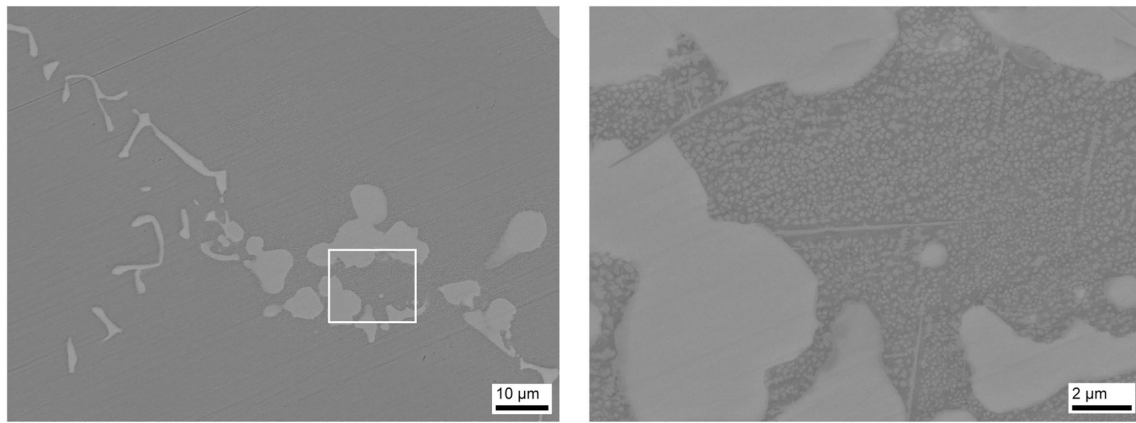


Fig. 5 Interdentritic area precipitates in the as-cast material. γ' precipitates were found in close vicinity of MC carbides. Plate-shaped particles growing out of MC particles are presumed to be η phase

explain the high hardness of the alloy in the as-cast condition. It has to be noted, however, that the γ' precipitation is not uniform but rather concentrated close to interdendritic areas around larger Nb-rich precipitates, where their particle size increased as well. Small plate-like precipitates can also be observed in close vicinity to the Laves phase/MC carbides. The morphology suggests η phase, which has been reported in ATI 718Plus® [11]. While qualitative distinction was possible from SEM images, the phases were too small for EDS analysis.

With the preliminary assumption that both Laves phase and MC carbides are present in the as-cast microstructure, XRD scans were conducted on electrolytic phase extracts of different heat treatment conditions to confirm the dissolution of interdendritic precipitates. Figure 6 shows the results from XRD analysis with indexed peaks for the C14 Laves phase (P63/mmc, 194), NbC (Fm3m, 225) and γ' (Pm3m, 221). While the spectra for the as-cast condition and the 1120 °C 4 h solution heat treatment show identical peak positions for NbC and Laves, the Laves phase peaks disappear for the

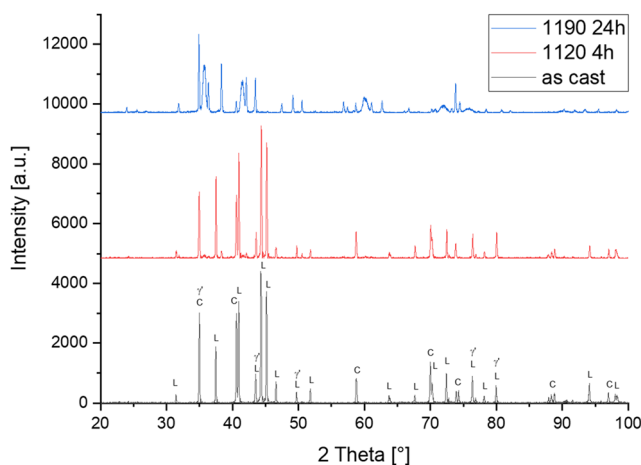


Fig. 6 XRD spectra on extracted powder of ATI 718Plus® in the as-cast condition (bottom) and after homogenisation heat treatments at 1120 °C 4 h (middle) and 1190 °C 24 h (top). The Laves phase peaks are absent in the latter condition

1190 °C 24-h heat treatment. Additionally, significant peak shift and peak broadening can be observed. The η phase could not be identified with powder XRD, presumably owing to its relatively small phase fraction and the difficulty to distinguish phases with similar crystal structures with only small differences in lattice parameter. The η phase has a hexagonal P63/mmc, 194 crystal structure [11], which is similar to the more abundant Laves phase. Furthermore, the used filter size of 0.8 μm together with the small phase fraction and size of the presumed η precipitates shown in Fig. 5 makes it possible that they were not filtered out from the extraction solution.

TEM SA diffraction was used together with TEM EDS to confirm the phases present in the material. This part of the investigation was conducted on the as-cast condition, presuming that all phases observed with the SEM and XRD had the highest phase fractions in this material condition. Figure 7, 8 and 9 show TEM bright field and dark field images of the phases found in the material, together with their respective SA diffraction patterns and TEM EDS spectra. Quantitative TEM EDS results are presented in Table 3.

For the phase shown in Fig. 7, it can be observed that, apart from having a relatively large size, a clear peak on the Nb L- α position is present in the EDS spectrum. The diffraction patterns shown in Fig. 7c–e were indexed as a cubic Fm3m (225) crystal structure. This confirms the particle as Nb(Ti) MC-type carbide.

A phase showing EDS spectra with peaks at the Nb-L α and Mo-L α positions was also found during TEM analysis. Apart from the presence of other element signatures, the Nb intensity is significantly lower as compared with the Nb carbide shown in Fig. 8a, suggesting a different phase. SA diffraction analysis revealed a hexagonal crystal structure typical for the C14 Laves phase. Together with the TEM EDS results shown in Table 3, this supports the findings of both the SEM and XRD results, where similar EDS and crystallographic signatures were observed.

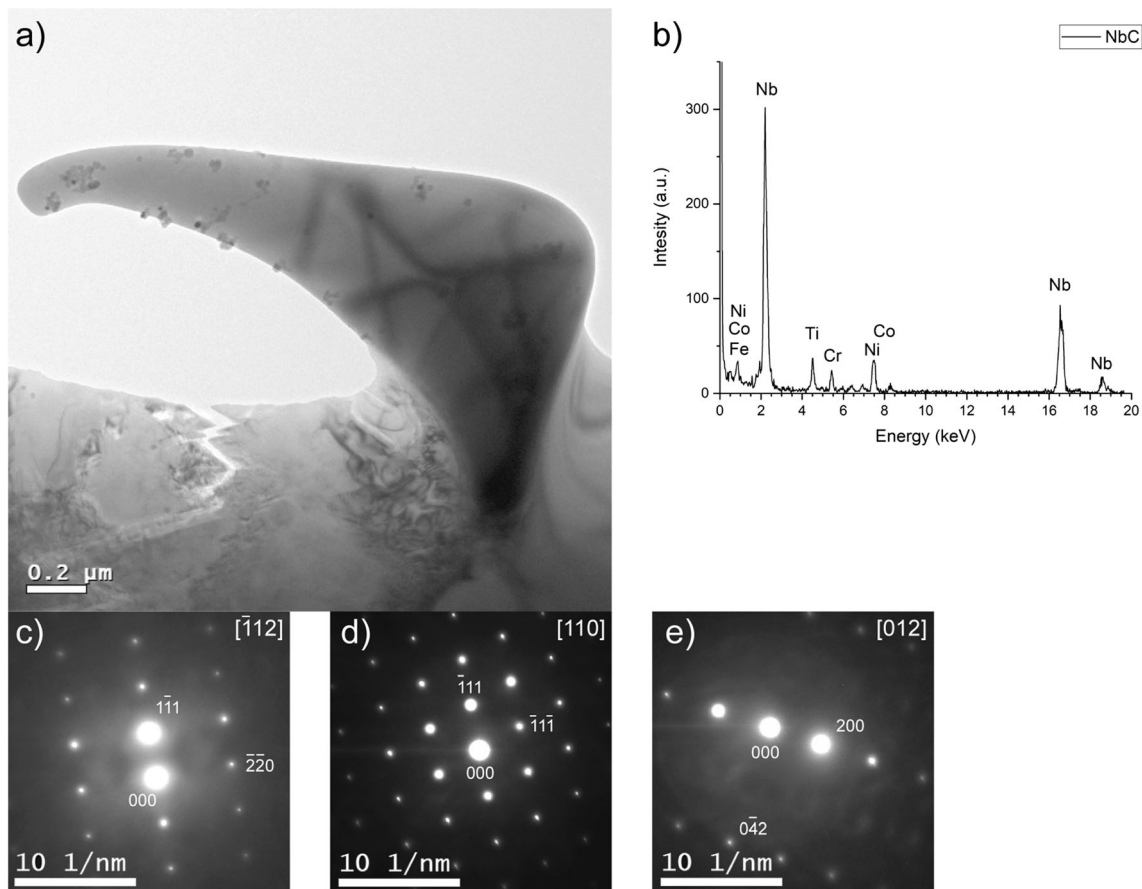


Fig. 7 TEM bright field image of a Nb(Ti) MC-type carbide (a), with TEM EDS showing high intensity at the Nb-Lx position (b). SA diffraction patterns are shown indexed as cubic Fm3m structure with $[112]$ (c), $[110]$ (d) and $[012]$ (e)

In the surroundings of the Laves phase, cuboidal γ' precipitates were found as well, which are shown as $\langle 110 \rangle$ dark field image in Fig. 9a together with the respective SA diffraction pattern in Fig. 9b, where the γ' sublattice reflections are clearly visible. The particles were found to have a maximum particle size of about 120 nm. As observed in the SEM investigation (cf. Fig. 5), the phase is however not uniformly present in the material and instead is only found surrounding in interdendritic precipitates. The presented maximum particle radius does not represent the total population of γ' particles. Nevertheless, their presence explains the high hardness of the as-cast condition as compared with the homogenisation heat-treated material.

3.2 Weld cracking

The difficult-to-weld groove geometry with a small bottom radius, together with a relatively high heat input as compared with typical repair welding operations produced weld cracks in all tested conditions. Cracks were found in both fusion zone (FZ) and HAZ as presented in Fig. 10a, b. Fusion zone cracking did not show a clear trend with changing base material microstructure, and the total crack length in the fusion zone was found to be generally lower than those observed in the HAZ. It can be

reasonably assumed that cracking in the FZ was mostly affected by the heat input and thermal stresses generated during the welding operation. The presented results have not been normalised with respect to investigated cross-section area, which was larger for the FZ with a factor of approximately 3:1. Higher total crack length in the HAZ, combined with the smaller investigated cross-section area indicates that HAZ cracking is the more severe cracking phenomenon in this material. Furthermore, with cracking occurring in the base material, an effect of pre-weld thermal history can be observed. Both the as-cast condition and homogenisation heat treatment at 1120 °C for 4 h produced a comparable TCL. All other heat treatments resulted in an increased TCL in the HAZ.

Microstructural characterisation revealed a difference in crack appearance, with short cracks for as-cast and 1120 °C 4 h, while long cracks running along former solidification grain boundaries were found for the other homogenisation heat treatments. Using average crack length values instead of the TCL confirms the results of visual microstructural inspection as indicated in Fig. 11.

The homogenisation heat treatments were most discernible by the amount of the Laves phase they could dissolve (cf. Fig. 2 and 3). With the absence of high-Nb, low melting phases in the

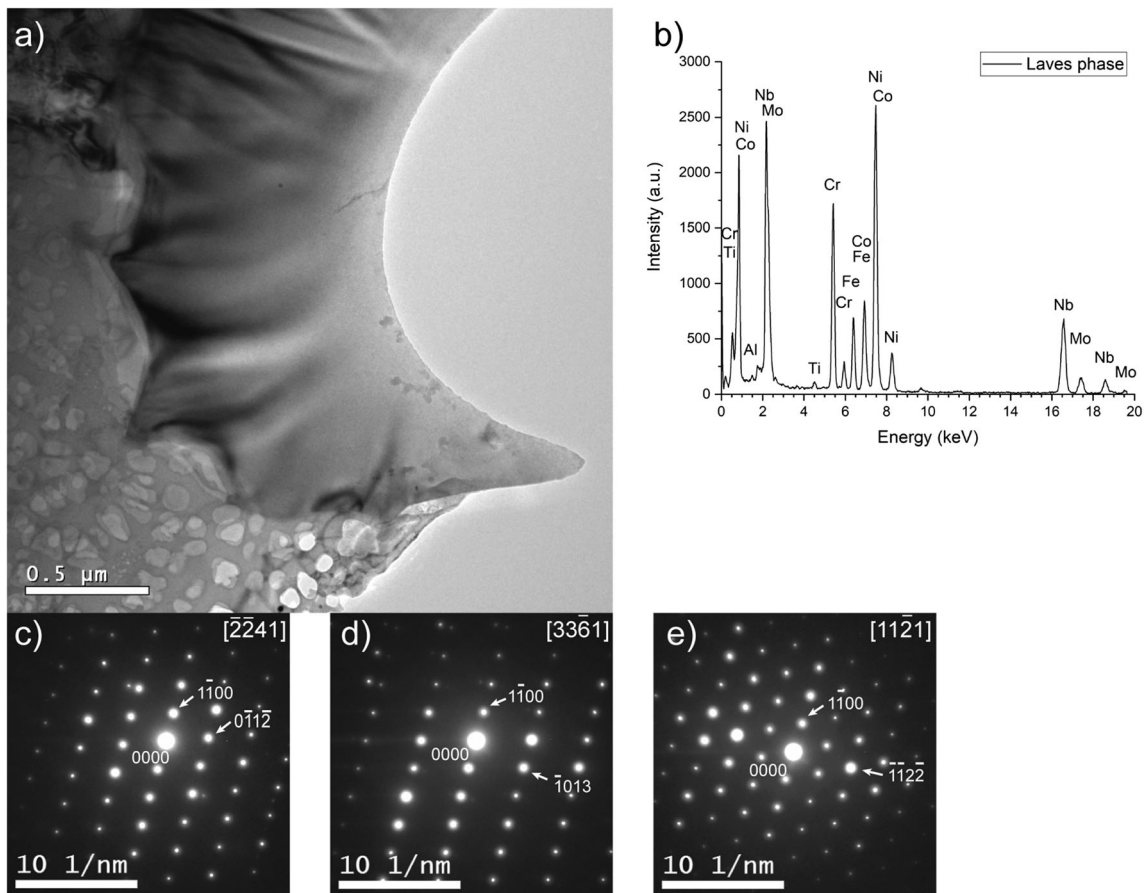


Fig. 8 TEM bright field image of the Laves phase particle (a), with TEM EDS showing high presence of Nb, Mo and Cr. SA diffraction patterns are shown indexed as hexagonal P63/mmc structure with $[2\bar{2}41]$ (c), $[3\bar{3}61]$ (d) and $[11\bar{2}1]$ (e)

microstructure, long cracks were formed on former solidification grain boundaries, while the Laves phase containing samples produced shorter cracks. The typical crack appearance is shown in

Fig. 12, exemplarily for samples homogenised at 1120 °C for 4 h and 1190 °C for 24 h, respectively. The former also shows significant Laves liquation in the HAZ in the form of fine gamma-

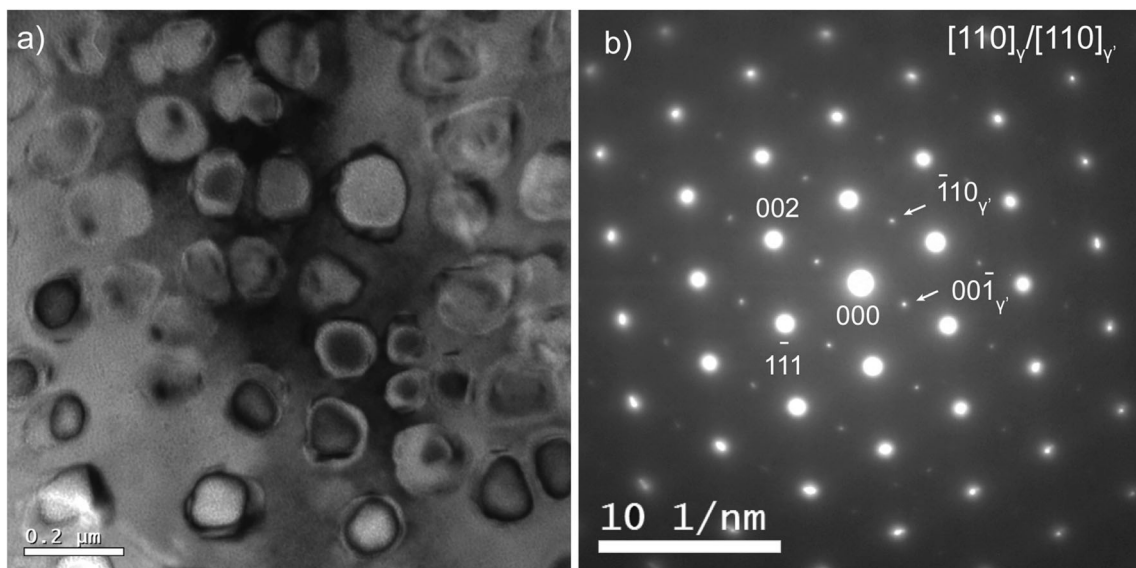


Fig. 9 a TEM $\langle 110 \rangle$ dark field image of cuboidal γ' particles surrounding laves phase. b The SA diffraction pattern clearly reveals the γ' sublattice reflections

Table 3 TEM EDS results of matrix, NbC and Laves phase in wt%

	Al	Ti	Cr	Fe	Co	Ni	Nb	Mo	W
Matrix	1.27	0.96	20.85	8.67	7.84	51.49	6.55	2.37	0
NbC	0	5.23	4.03	1.11	1.41	10.71	77.51	0	0
Laves	0.44	0.57	15.78	6.16	8.68	33.63	27.61	5.84	1.29

Laves eutectics in interdendritic areas and around the formed cracks. Cracks formed in interdendritic areas are furthermore forced to propagate following the shape of the dendrites, which causes a tortuous appearance. Cracks in the Laves-free material on the other hand propagate on relatively straight solidification grain boundaries. Grain boundary tortuosity has been found to reduce ductility-dip cracking in high-Cr filler metals due to hindering crack propagation [12], which can be assumed to also contribute to the shorter observed crack lengths in the Laves-containing material.

3.3 Liquation mechanism for HAZ liquation cracking

A typical marker for re-solidified liquid in Nb-bearing alloys is the presence of the gamma-Laves eutectic. Microstructural investigation of HAZ cracks found in material without the Laves phase being present before welding did not always show clear signs of liquation. Thermal cycles were not measured during the welding operation, and the manual nature of the process makes it difficult to identify the conditions and the mechanism that caused crack formation. Gleeble thermomechanical simulations were therefore used to provide a controlled environment for studying the microstructural development under short-time high temperature exposure. The thermomechanical simulations produced cracks comparable with those found in the repair welds. Homogenisation at 1120 °C for 4 h shows a slightly higher stress to fracture (30 vs 25 MPa) than the material homogenised at

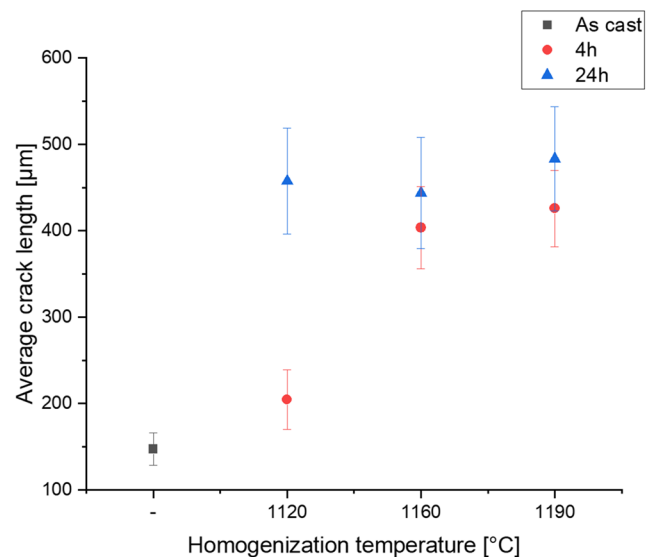


Fig. 11 Average crack length in the base metal HAZ of as cast and homogenised ATI 718Plus[®], showing significantly lower values for material in the as-cast condition and after 1120 °C 4 h homogenisation heat treatment

1190 °C for 24 h when tested in the hot ductility test at 1150 °C. The fracture and associated ductility, Fig. 13, is zero for both material conditions at this test temperature, indicating significant liquation. The fracture surfaces resemble the general microstructural appearance after homogenisation heat treatment. Lower homogenisation temperature and exposure time retained a more dendritic structure, while at 1190 °C, those cast features are much less visible. This led to a more dendritic fracture surface appearance with smaller features for the lower homogenisation temperature, however both samples show similar signs of liquation in the form of small freckles on the surface of grain and dendrite facets.

To confirm microstructural evolution during fast heating, a set of samples was thermally cycled without externally applied

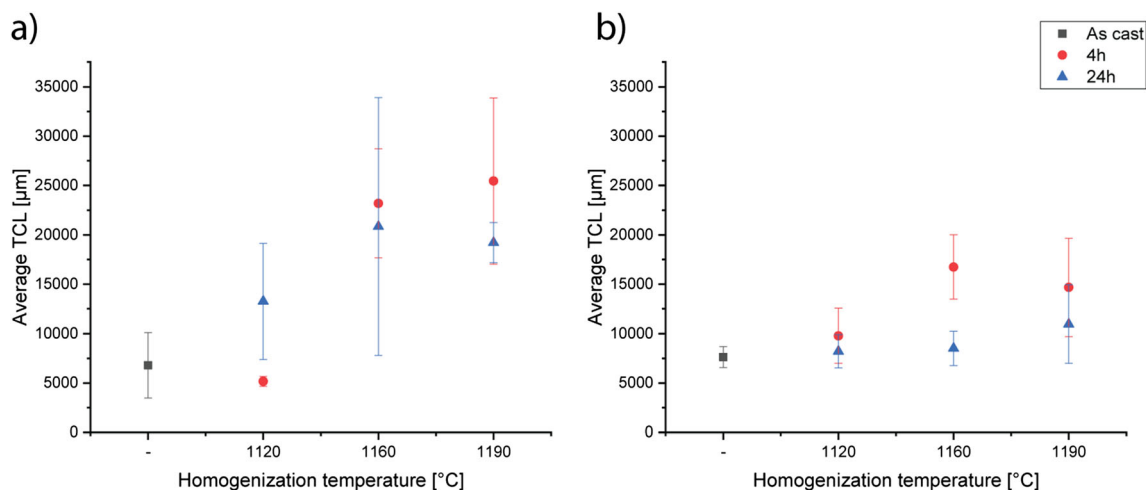


Fig. 10 Total crack length in (a) HAZ and (b) FZ after welding as a function of pre-weld homogenisation heat treatment condition

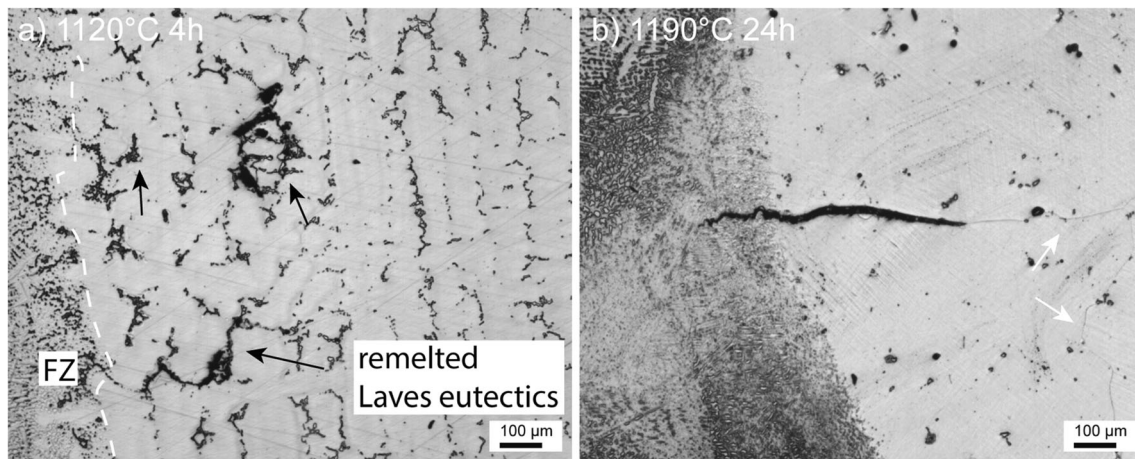


Fig. 12 Crack appearance in the base metal HAZ. **a** Short, not connected cracks in interdendritic regions of material homogenised at 1120 °C for 4 h. The fusion zone boundary is indicated by dashed line, while arrows

indicate fine eutectic structure of the remelted Laves phase. **b** 1190 °C 24 h homogenisation heat treatment showing a long crack running along a former solidification grain boundary (indicated by arrows)

load. However, even under this test condition, the material homogenised at 1190 °C for 24 h fractured upon thermal exposure at 1150 °C. Figure 14 shows one of the formed cracks propagating along a former solidification grain boundary. Indicated are also two NbC carbide particles showing signs of constitutional liquation in the form of gamma-Laves eutectic around the carbide particles. One of them is located on the fractured grain boundary, and it is evident that the gamma-Laves eutectic liquid spread onto the surrounding grain boundary area. Spot EDS analysis revealed a similar chemical composition as those determined with TEM measurements, cf. Table 3.

Nb(Ti) MC-type carbides have been confirmed to be present in the microstructure of the material by both TEM and phase extraction XRD analysis. The presence of the gamma-Laves eutectics around those particles suggests that a liquation mechanism is constitutional liquation. The presence of precipitates on solidification grain boundaries can explain the high sensitivity of the material to HAZ liquation cracking since formed liquid can spread over a large area, lowering the

materials' load bearing capabilities. The Laves phase dissolution during homogenisation heat treatments causes a locally increased Nb concentration. While the concentration is expected to approach that of the nominal alloy composition during homogenisation heat treatment, higher than nominal Nb concentrations can suppress the melting point of the matrix. When assuming that the liquation due to Nb segregation can be described by a pseudo-binary phase diagram [13], the Laves eutectic temperature is the lowest possible melting temperature. While the presence of Laves phase hence can be expected to cause the presence of large amounts of liquid phase over a wider temperature range, higher Nb concentrations can increase the likelihood of constitutional liquation to occur, since less Nb has to be released from carbides to reach the critical composition for the formation of the gamma-Laves eutectics.

High homogenisation heat treatments and their associated cooling cycles have been found to create an environment where non-equilibrium boron segregation can occur at grain boundaries in Alloy 718 and ATI 718Plus® [14, 15]. This in

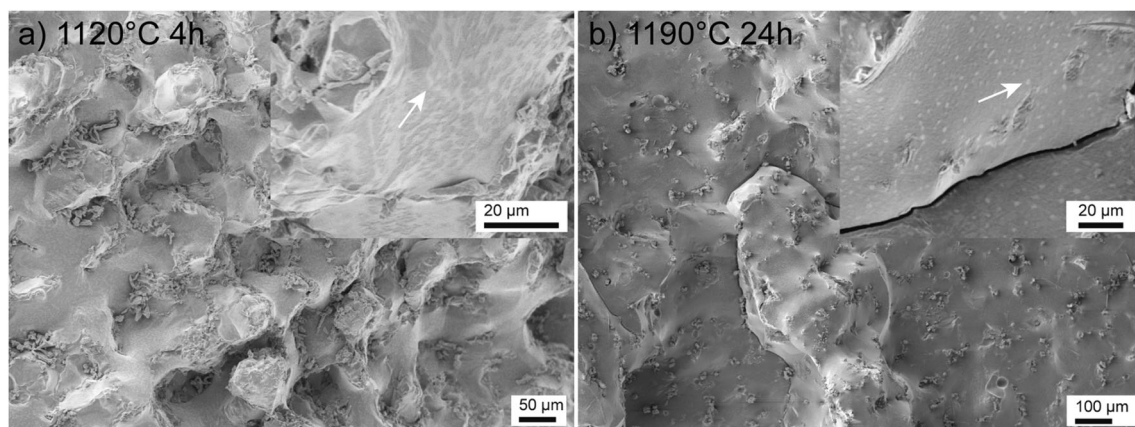


Fig. 13 Fracture surfaces after thermomechanical Gleeble simulation at 1150 °C on microstructures with (a) 1120 °C 4 h and (b) 1190 °C 24 h homogenisation heat treatment. Signs of liquation are indicated by arrows

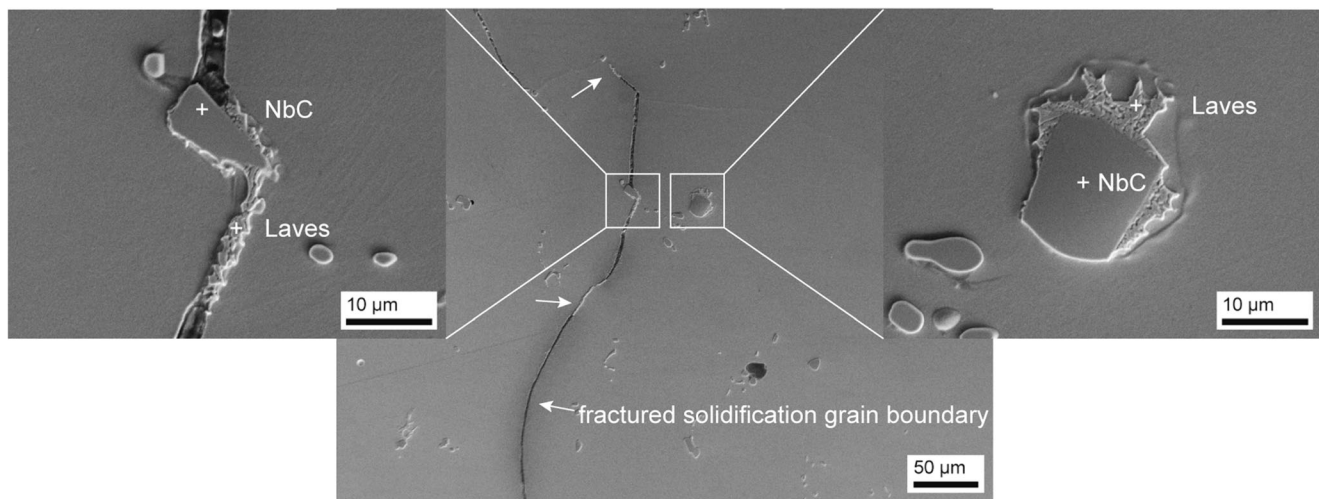


Fig. 14 Cracked grain boundary in Gleeble-simulated HAZ microstructure with Nb(Ti) MC-type carbides lying on and in close vicinity to the grain boundary. Presence of the γ -Laves eutectic surrounding the

particles indicates the formation of liquid. Presence of further gamma-Laves eutectic is indicated by right facing arrows

turn can lead to local melting point suppression and the formation of liquid during subsequent high temperature exposure. Without further investigation using, e.g. secondary-ion mass spectroscopy (SIMS), this liquid formation mechanism cannot be confirmed for ATI 718Plus® in the present study. The boron content of the studied cast alloy can however be compared with the high boron heat investigated by Vishwakarma and Chaturvedi [15], suggesting the presence of this type of liquation mechanism in the material. Boron increases the grain boundary wetting behaviour [16] and could hence contribute to the distribution of liquid formed due to segregation of Nb. Non-equilibrium segregation of boron however could not completely explain the negative effect of longer exposure time at 1120 °C, since the segregation of boron occurs during cooling after the heat treatment and should hence be independent of exposure time. Equilibrium segregation of boron has been found to be the dominating segregation mechanism at temperatures below approximately 1100 °C for Alloy 718 [14], leaving the possibility that equilibrium segregation of boron contributes to the higher cracking susceptibility of the 1120 °C 24 h samples.

The relative resistance of material with the residual eutectic gamma-Laves can be correlated to the extensive formation of liquid caused by liquation during high temperature exposure. The relative abundance of the Laves phase in the as-cast and 1120 °C 4 h homogenisation material condition produces a large amount of liquid during welding. The presence of thin liquid films has been reported to promote HAZ liquation cracking [17], while increased liquation was found to lower cracking [18]. Ojo and Chaturvedi discuss the effect of liquid film thickness by applying solidification cracking theories such as Borland's generalized theory and Pellini's theory of hot tearing [19–21], where increased film thickness is attributed to a lower risk crack formation due to increased mobility

of the liquid and the surrounding solid material. With Nb(Ti) MC-type carbides present in all studied material conditions, their liquation during welding can be assumed to be present irrespective of the thermal history. The formation of high amounts of liquid in not completely homogenised material as visible in Fig. 12a however appears to better accommodate stresses generated in the material during cooling from the weld thermal cycle, which contributes to a higher HAZ cracking resistance.

4 Conclusions

The microstructural evolution of cast ATI718Plus® subjected to different homogenisation heat treatments has been studied. Secondary phases present in the as-cast condition could be identified as Nb(Ti) MC-type carbides and C14 Laves phase. All homogenisation heat treatments but 1120 °C 4 h were able to completely dissolve the Laves phase.

The weld cracking response was strongly affected by base material microstructure, with the Laves phase containing microstructures showing a higher resistance to HAZ cracking as compared with the material where the Laves phase was completely dissolved during homogenisation heat treatment. Constitutional liquation could be identified as one of the liquation mechanisms in Laves-free material, where gamma-Laves eutectic has been found on former solidification grain boundaries around Nb(Ti) MC-type carbides. The large grain boundary area of those grain boundaries allows for the formation of long cracks in the base metal HAZ. Boron segregation could further enhance wetting behaviour and the spreading of liquid along solidification grain boundaries. While constitutional liquation is a possible liquation mechanism in all material condition due to the presence of Nb(Ti) MC-type carbides,

a high phase fraction of Laves phase was found to lower HAZ cracking by forming thick liquid films. The abundance of liquid in the HAZ has been connected to an increased capability of the material to relax weld thermal stresses. The localization of cracks in interdendritic areas furthermore forces cracks to follow the tortuous shape of dendrite arms, hindering crack propagation. While cracking in Laves-free material is connected to constitutional liquation of Nb(Ti) MC-type carbides and boron segregation, the dominant liquation mechanism in microstructures containing Laves phase is the formation of gamma-Laves eutectics. The formation of large amounts of liquid and crack localisation in interdendritic areas links the presence of the Laves phase to an increased HAZ cracking resistance.

As-cast and 1120 °C 4 h homogenised materials showed the highest weld cracking resistance, indicating that carrying out homogenisation heat treatments after welding operations could reduce weld cracking in the material. While this is not a feasible approach for the production of components, such a method could be applied to reduce weld cracking in the material when repairing cast structures.

Acknowledgements The authors sincerely acknowledge Roland Stridh and Patrik Karlsson from GKN Aerospace Sweden AB for carrying out the repair welding operations and thank Kathrin Dalberg and Linn Myrthil Skagerlind for their help with the evaluation process. Asala Gbenga from the University of Manitoba is acknowledged for his help with TEM sample preparation and fruitful discussions.

Funding information Open access funding provided by Chalmers University of Technology. The support by the Consortium Materials Technology for Thermal Energy Processes (KME) through funding from Swedish Energy Agency and GKN Aerospace Sweden AB is highly appreciated.

Open Access This article is licensed under a Creative Commons Attribution 4.0 International License, which permits use, sharing, adaptation, distribution and reproduction in any medium or format, as long as you give appropriate credit to the original author(s) and the source, provide a link to the Creative Commons licence, and indicate if changes were made. The images or other third party material in this article are included in the article's Creative Commons licence, unless indicated otherwise in a credit line to the material. If material is not included in the article's Creative Commons licence and your intended use is not permitted by statutory regulation or exceeds the permitted use, you will need to obtain permission directly from the copyright holder. To view a copy of this licence, visit <http://creativecommons.org/licenses/by/4.0/>.

References

1. Cao WD, Kennedy R (2004) Role of chemistry in 718-type alloys - Allvac 718Plus development. In: Proceedings of the 10th international symposium on Superalloys
2. Peterson B, Krishnan V, Brayshaw D, Helmink R, Oppenheimer S, Ott E, Benn R, Uchic M (2010) Castability of 718Plus® alloy for structural gas turbine engine components. In: Proceedings of the 7th International Symposium on Superalloy, pp 131–146

3. Peterson B, Frias D, Brayshaw D, Helmink R, Oppenheimer S, Ott E, Benn R, Uchic M (2010) On the development of cast ATI 718Plus® alloy for structural gas turbine engine components. In: Proceedings of the 7th International Symposium on Superalloy, pp 787–794
4. DuPont JN, Lippold JC, Kiser SD (2009) Welding metallurgy and weldability of nickel-base alloys. Wiley, Hoboken, N.J
5. Andersson J, Sjöberg G, Larsson J (2010) Investigation of homogenization and its influence on the repair welding of cast Allvac 718Plus. In: Proceedings of the 7th International Symposium on Superalloy 718 and Derivatives, pp 439–454
6. Hanning F, Andersson J (2018) The influence of base metal microstructure on weld cracking in manually GTA repair welded cast ATI 718Plus®. In: Proceedings of the 2018 Superalloy 718 & Derivatives: Energy, Aerospace, and Industrial Applications, Pittsburgh, USA, vol 9, pp 917–928
7. Andersson J, Sjöberg G, Hänninen H (2011) Metallurgical response of electron beam welded Allvac 718Plus™, in hot cracking phenomena in welds III. Springer, Berlin Heidelberg, pp 415–429
8. Practice for electrolytic extraction of phases from ni and ni-fe base superalloys using a hydrochloric-methanol electrolyte, ASTM International, West Conshohocken, PA, ASTM E963–95
9. Andersson J, Sjöberg G, Chaturvedi M (2010) Hot ductility study of HAYNES 282 superalloy. In: Proceedings of the 7th International Symposium on Superalloy 718 and Derivatives, pp 539–554
10. Cao W-D (2005) Solidification and solid state phase transformation of Allvac 718Plus Alloy. In: Superalloys 718, 625, 706 and Various Derivatives (2005), pp 165–177
11. Pickering EJ, Mathur H, Bhowmik A, Messé OMDM, Barnard JS, Hardy MC, Krakow R, Loehnert K, Stone HJ, Rae CMF (Apr. 2012) Grain-boundary precipitation in Allvac 718Plus. *Acta Mater* 60(6–7):2757–2769
12. Ramirez AJ, Lippold JC (Aug. 2004) High temperature behavior of Ni-base weld metal part II – insight into the mechanism for ductility dip cracking. *Mater Sci Eng A* 380(1–2):245–258
13. Andersson J, Raza S, Eliason A, Surreddi KB (2014) Solidification of alloy 718, ATI 718Plus and waspalloy. In: Proceedings of the 8th International Symposium on Superalloy 718 and Derivatives, pp 181–192
14. Huang X, Chaturvedi MC, Richards NL, Jackman J (Aug. 1997) The effect of grain boundary segregation of boron in cast alloy 718 on HAZ microfissuring—a SIMS analysis. *Acta Mater* 45(8):3095–3107
15. Vishwakarma KR, Chaturvedi MC (Mar. 2009) Effect of boron and phosphorus on HAZ microfissuring of Allvac 718 Plus superalloy. *Mater Sci Technol* 25(3):351–360
16. Kelly TJ (1989) Elemental effects on cast 718 weldability. *Welding J* 68(2):44s–51s
17. Owczarski WA, Duvall DS, Sullivan CP (1966) A model for heat-affected zone cracking in nickel-base superalloys. *Weld. J.* 45(4):145s–155s
18. Idowu OA, Ojo OA, Chaturvedi MC (Apr. 2007) Effect of heat input on heat affected zone cracking in laser welded ATI Allvac 718Plus superalloy. *Mater Sci Eng A* 454–455:389–397
19. Ojo OA, Chaturvedi MC (Mar. 2007) Liquation microfissuring in the weld heat-affected zone of an overaged precipitation-hardened nickel-base superalloy. *Metall Mater Trans A* 38(2):356–369
20. Borland JC (Aug. 1960) Generalized theory of super-solidus cracking in welds (and castings). *Br Weld J* 7(8):508–512
21. Pellini WS (1952) Strain theory of hot tearing. *Foundry* 80(11):125–133;192–199

Publisher's note Springer Nature remains neutral with regard to jurisdictional claims in published maps and institutional affiliations.